PAPER

Check for updates

Adsorption and photo-Fenton catalytic degradation of organic dyes over crystalline LaFeO₃-doped porous silica†

Thi To Nga Phan, Aleksandar N. Nikoloski, Parisa Arabzadeh Bahri and Dan Li [iD] *

LaFeO₃ (LFO)-doped mesoporous silica (HPS) (HPS-xLFO with theoretical LFO/silica molar ratio $x = 0.075$, 0.15, 0.3) was successfully prepared *via* impregnation of metal ions into the porous silica HPS-0LFO support and subsequent calcination. The characterization studies suggest that increasing the doping of LFO, which exhibited a particle size of ~10–15 nm, in the silica support led to a reduction in surface area and bandgap of the resulting catalyst. The use of HPS-0.15LFO yielded a superior removal rate (98.9%) of Rhodamine B (RhB), thanks to the effective dark adsorption and visible light-induced photo-Fenton degradation, both of which were greater than those of pure LFO crystals. This enhancement could be explained by the unique properties of the mesoporous silica support. In particular, the wide-opening mesopores created a large surface area to dope LFO as active sites and minimize diffusion of RhB into pores during the photo-Fenton reaction. The photo-Fenton catalytic degradation of RhB could reach 98.6% within 90 min exposure to visible light irradiation under optimized conditions: RhB concentration = 10 mg L^{-1}, catalyst dosage = 1 g L^{-1}, pH = 6 and H₂O₂ = 15 mM. Moreover, the recycle and reuse test proved the good stability and repetitive use of HPS-0.15LFO for high performance RhB removal.

1. Introduction

Advanced oxidation processes (AOPs) have been considered as alternative and effective methods in treating various industrial wastewaters contaminated by dyes and organic compounds over the last few years. As one of the AOPs, the Fenton reaction, using the strong oxidant hydrogen peroxide to generate highly reactive hydroxyl radicals (˙OH), has attracted intensive research interest since the 1960s in the removal of a variety of recalcitrant organic contaminants.[1] Typically, the Fenton process is conducted in a homogeneous way using dissolved ferrous ions and hydrogen peroxide as Fenton reagents. However, the application of the homogeneous Fenton process on an industrial scale is limited due to: (i) pH-dependent chemical reactivity of iron; (ii) difficulty and complexity in separation and recovery of metal ions from the final effluent.[2] Therefore, research efforts have been directed towards designing heterogeneous iron-based Fenton-like catalysts, such as iron oxide,[3] iron exchanged zeolite[4] and iron supported

porous material.[5] Combined with visible light irradiation, the cost-effectiveness of a heterogeneous Fenton-like process for use in wastewater treatment has been seen as promising.[6,7]

Perovskite materials having the generic formula of ABO₃, in which A is typically an alkaline-earth or rare-earth element and B is a transition metal, have been found to exhibit high visible light photo-Fenton-like activity for dye degradation.[8,9] Ju *et al.* found that EuFeO₃ nanoparticles prepared by the sol–gel method and calcined at 750 °C yielded 71% removal rate in 5 mg L^{-1} Rhodamine B (RhB) solution after being exposed to visible light for 3 h, in the presence of 1 g L^{-1} catalyst and 0.05 mL H₂O₂.[8] An and co-workers investigated the use of BiFeO₃ heterogeneous photo-Fenton-like catalyst synthesized by the sol–gel method on the degradation of RhB, Methyl Violet (MV) and phenol.[9] Their results revealed that with the assistance of visible light irradiation, the RhB, phenol and MV degradation rate constant (k), derived from the pseudo-first-order model, was increased by 1.95, 2.07 and 3.47 times, respectively, compared to that under the dark condition. The utilization of visible light enhanced the photocatalytic activity of BiFeO₃ for pollutant degradation in the presence of H₂O₂.

The literature suggests that LaFeO₃ (LFO), as a member of the group of perovskite materials, could be a promising heterogeneous catalyst in the photo-Fenton degradation of pollutants.[10–13] In the photo-Fenton reaction, the pollutant is believed to be oxidized and degraded by the attack of the hydroxyl radicals; thereby it is necessary to increase the number of active sites on the catalyst surface and in turn enhance the

Chemical and Metallurgical Engineering and Chemistry, School of Engineering and Information Technology, Murdoch University, Western Australia, Australia. E-mail: L.Li@murdoch.edu.au; Tel: +61 8 9360 2569

contact area between the pollutant and the catalyst towards the optimization of pollutant removal. However, LFO crystals synthesized *via* the traditional sol–gel method normally possess small specific surface area, show no porosity and therefore have a limited amount of active sites for catalytic degradation,[10,14] due to the high temperature usually used in the synthesis.

So far, there has been some effort contributed to the development of supported LFO catalysts with porosity for high-performance Fenton or photo-Fenton degradation of pollutants. A number of materials have been explored for use as the supports, such as montmorillonite,[15] carbon spheres,[16] mesoporous silicas,[17,18] and graphene.[19] In particular, mesoporous silicas have received recent research interest because of their unique features, including high specific surface area, tunable pore size and structure.[20–23] Zhu's group successfully loaded LFO on SBA-15 mesoporous silica and investigated its Fenton-like catalytic activity for the oxidation of Rhodamine B (RhB), reactive brilliant red X-3B, direct scarlet 4BS and methylene blue (MB).[17] The results showed that 80% and 66% of RhB and MB was removed after 60 min, respectively; whilst that for 4BS and X-3B was similar, approximately 42% (test conditions: 1 mL of 30 wt% H_2O_2, 0.1 g catalyst and 50 mL of 0.02 mmol L^{-1} dye solution). It was also concluded that SBA-15-supported LFO was more efficient than the bulk LFO in the catalysing oxidation of organic. Later the same group studied the role of silica, including porous (*e.g.* SBA-15, SBA-16, MCF) and non-porous silica powders, on RhB oxidative degradation using the supported LFO.[24] Their results revealed that the LFO sample supported by MCF, which had randomly distributed pores and short pore length, exhibited the highest photocatalytic performance when compared to other LFO-doped samples. This suggests that the porous structure of the support plays an essential role in the adsorption of the organic, its transportation to active sites and eventually catalytic degradation.[24] However, there have been few publications, exploring the use of silica-supported LFO for enhanced photo-Fenton degradation of organics under visible light irradiation. There have been no reports of studies to optimize its catalytic performance under different operational conditions or to investigate its feasibility for recycle and reuse; all of which is necessary information for practical utilization in wastewater treatment.

In this work, a type of mesoporous silica (HPS), which showed a unique fine pore system, narrow inner channels and wide outer pore opening,[25] was selected as a support for different amounts of LFO doping to prepare heterogeneous photo-Fenton-like catalysts HPS-*x*LFO (with theoretical LFO/silica molar ratio *x* = 0.075, 0.15, 0.3). This unique mesoporous structure may endow great surface area for LFO doping and in turn would offer a large number of active sites. Meanwhile, its wider pore opening would greatly reduce the resistance to large organic molecules being transported into the pores and reaching active sites for catalytic degradation. RhB, a representative of xanthane dyes, is widely used in a variety of industries (*e.g.* textile, dyeing, paint and printing) and imposes hazardous effect on the environment and public health.[26,27] Although significant effort has been concentrated on the application of methods, including adsorption,[28] membrane

separation,[29] ion flotation[30] and ozonation,[31] to remove RhB from water, they have to date been found to be ineffective or uneconomical due to the stability of dye.[26] In this study, we selected RhB as the model organic dye to investigate its removal effectiveness using HPS-*x*LFO *via* adsorption and photo-Fenton catalytic degradation. The effect of catalyst dosage, H_2O_2 concentration, solution pH and co-existing ions on the photo-Fenton removal of RhB was investigated; and its performance after recycling was also studied.

2. Experimental

2.1 Chemicals

Cyclohexane (C_6H_{12}; 99.9%), 1-pentanol ($CH_3(CH_2)_4OH$; ≥99%), cetyltrimethylammonium bromide ($CH_3(CH_2)_{15}$-$N(Br)(CH_3)_3$; 99%), tetraethyl orthosilicate ($Si(OC_2H_5)_4$; 99%), lanthanum nitrate hexahydrate ($La(NO_3)_3 \cdot 6H_2O$; 99.9%), citric acid ($C_6H_8O_7 \cdot H_2O$; ≥99.5%), H_2O_2 (30 wt%), and Rhodamine B (RhB; ≥95%) were purchased from Sigma-Aldrich. Iron nitrate nonahydrate ($Fe(NO_3)_3 \cdot 9H_2O$; 98–101%) was purchased from Alta Aesar. Urea (NH_2CONH_2) was obtained from Merck Pty Limited, Australia. Other chemicals were from Biolab Ltd in Australia. All of the chemicals were used without additional purification.

2.2 Preparation of porous silica

Mesoporous silica (HPS-0LFO) support was synthesized according to a reported procedure.[25] First of all, 2.7 mL tetraethyl orthosilicate (TEOS) was dissolved in the mixture with 1.5 mL 1-pentanol and 30 mL cyclohexane at the room temperature. The resulting solution was stirred for 5 h, followed by the addition of a mixture which was made up of 1.87 g cetyltrimethylammonium bromide (CTAB), 0.6 g urea, 30 mL deionized (DI) water. After stirring, the solution was transferred into a Teflon-lined autoclave (100 mL) and heated in an oven at 120 °C for 4 h. Finally, white precipitates were separated from the liquid, washed with acetone and DI water, dried in an oven and calcined in air at 550 °C for 6 h (heating rate of 1 °C min^{-1} from room temperature to 550 °C).

2.3 Synthesis of LaFeO₃-doped HPS

LaFeO$_3$-doped mesoporous silica (HPS-*x*LFO) was synthesized by impregnation and subsequent calcination. Typically, 10 mmol La(NO$_3$)$_3$·6H$_2$O, 10 mmol Fe(NO$_3$)$_3$·9H$_2$O and 20 mmol citric acid was dissolved in a mixture of 10 mL DI water and 20 mL of ethanol to form a homogeneous solution at room temperature. After adding 2 g HPS-0LFO, the resulting suspension was stirred at room temperature for 3 h and then at 70 °C to evaporate the solvent, followed by drying at 80 °C and then calcination at 700 °C (heating rate of 2 °C min^{-1} from room temperature to 700 °C). The theoretical molar ratio between LaFeO$_3$ (LFO) and silica in different samples was 0.075, 0.15 and 0.3. The corresponding catalysts were designated as HPS-0.075LFO, HPS-0.15LFO, and HPS-0.3LFO, respectively. For comparison, the sample, which was synthesized following

the same above procedures in the absence of HPS, was denoted as LFO.

2.4 Sample characterization

Powder X-ray diffraction (XRD) measurement was performed on a diffractometer (XRD, GBC eMMA), which was operated in the reflection mode with Cu Kα radiation (28 mA, 35 kV) at a step size of $1°$ min^{-1} in the range of 10–80°. The surface morphology and elemental composition of each sample was characterized using Scanning Electron Microscopy (SEM) (Zeiss 1555, VP-FESEM) at an accelerating voltage of 5 kV with energy dispersive X-ray spectrometry (EDS). The samples were loaded onto the carbon tape and coated by platinum. Transmission Electron Microscopy (TEM) analysis was performed on TEM-TITAN operating at 200 kV. The samples were dispersed in ethanol under ultrasonication and loaded onto carbon copper grid for TEM characterization. Nitrogen adsorption–desorption isotherms were measured at 77 K using SAPA2010 (Micromeritics Inc., USA). The samples were degassed at 200 °C overnight under vacuum.

2.5 Removal of RhB from water

100 mL of RhB aqueous solution (10 mg L^{-1}) was introduced into a cylindrical Pyrex vessel (300 mL), surrounded by a circulating water jacket to maintain solution temperature at 25 °C. 100 mg of HPS-xLFO ($x = 0$, 0.075, 0.15, 0.3) or 100 mg of LFO was added to the RhB solution; the resulting suspension was magnetically stirred in the dark for 90 min to investigate its adsorption of RhB in water. Samples were taken from the suspension at given period of times and centrifuged at 10 000 rpm. The obtained supernatant was analysed using a Perkin Elmer Lambda 750 UV/Vis spectrometer to determine the concentration of RhB (C_i, mg L^{-1}), compared to the initial concentration of RhB before adsorption (C, mg L^{-1}).

The results showed that the adsorption–desorption equilibrium was achieved within 30 min. Therefore, the photo-Fenton catalytic degradation test was started after 30 min dark adsorption using the catalyst. Typically, 100 mL of RhB aqueous solution (10 mg L^{-1}) was introduced into a cylindrical Pyrex vessel (300 mL), surrounded by a circulating water jacket to maintain solution temperature at 25 °C. 100 mg of HPS-xLFO ($x = 0$, 0.075, 0.15, 0.3) or LFO was added to the RhB solution; the resulting suspension was magnetically stirred in the dark for 30 min to reach adsorption–desorption equilibrium. After that, a xenon lamp (CEL-HX F300) with a 400 nm cut-off filter was used to provide visible light and 1 mL H_2O_2 was added to the suspension to initiate the photo-Fenton-like reaction. Samples were taken from the suspension at given periods of time and centrifuged at 10 000 rpm. The obtained supernatant was analysed using Perkin Elmer Lambda 750 UV/Vis spectrometer to determine the concentration of RhB (C_t, mg L^{-1}), as compared with the concentration of RhB before starting photo-Fenton-like degradation (C_0, mg L^{-1}).

The reusability of the catalyst was assessed by repeating the photo-Fenton degradation test under the same reaction conditions after recovering HPS-0.15LFO from the solution.

3. Results and discussion

3.1 Characterization of HPS-xLFO

The general morphologies of HPS-xLFO ($x = 0$, 0.075, 0.15, 0.3) with different LFO loadings are presented in Fig. 1. The sample of HPS-0LFO exhibited monodispersed spheres with a particle diameter of ∼300–400 nm. The morphology of LFO-loaded HPS (HPS-0.075LFO, HPS-0.15LFO, and HPS-0.3LFO) was similar to that of HPS-0LFO, suggesting that the HPS support is stable during doping with LFO. No significant LFO crystals or clumps were seen separately from the particles of HPS-xLFO ($x = 0.075$, 0.15, 0.3).

The morphology and size of HPS and HPS-0.15LFO observed by TEM (Fig. 2a and b) are consistent with those in Fig. 1. In Fig. 2a, the particles of HPS-0LFO exhibited a unique mesoporous structure. Compared with Fig. 2a, the TEM image of HPS-0.15LFO (Fig. 2b) shows that some small particles (*e.g.*
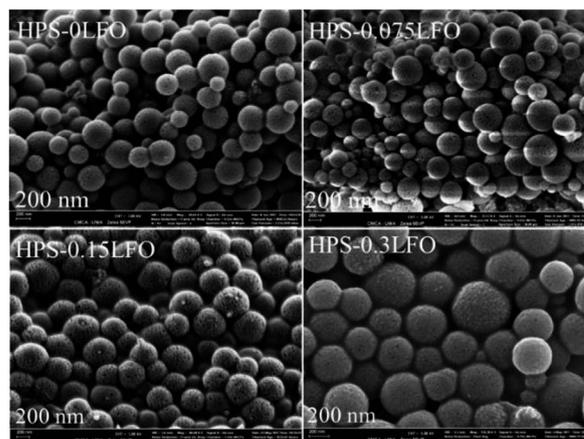

Fig. 1 SEM images of HPS-xLFO ($x = 0$, 0.075, 0.15, 0.3) samples.
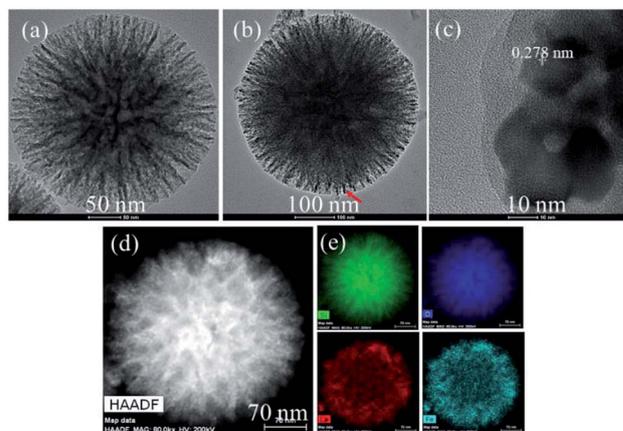

Fig. 2 TEM images of (a) HPS-0LFO and (b) HPS-0.15LFO; (c) HRTEM image of HPS-0.15LFO; (d) HAADF scanning TEM image of HPS-0.15LFO and (e) the corresponding elemental mapping (Si, O, La, and Fe).

indicated in red) were loaded in the HPS support. These particles were observed with an interplanar distance of 0.278 nm (Fig. 2c), which corresponds to the (121) crystal plane of LFO.[32] The high-angle-annular dark-field (HAADF) scanning TEM image of HPS-0.15LFO (Fig. 2d), and the corresponding elemental mapping images (Fig. 2e) further confirm that LFO was loaded to the HPS support.

The XRD patterns of HPS-xLFO (x = 0, 0.075, 0.15, 0.3) are shown in Fig. 3; the XRD pattern of LFO synthesized without the use of HPS was included for comparison. A broad characteristic peak at $2\theta = 23°$ was observed for the amorphous mesoporous SiO$_2$, HPS-0LFO. As expected, the LFO loading affected the porous structure of the HPS support. The characteristic peak intensity of SiO$_2$ considerably decreased with increased LFO loading in HPS, which is probably due to the partial or complete filling of LFO inside the HPS pores. The samples of HPS-0.075LFO, HPS-0.15LFO, and HPS-0.3LFO exhibited the characteristic diffraction peaks indexable to the orthorhombic structure of LFO (JCPDS no. 37-1493).[33] No apparent characteristic peaks of impurities were detected, confirming the high purity of the samples.
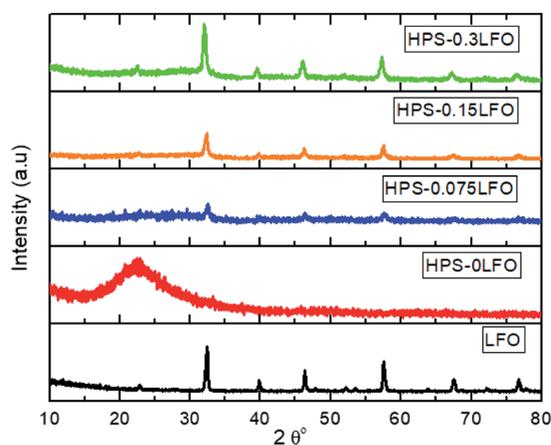

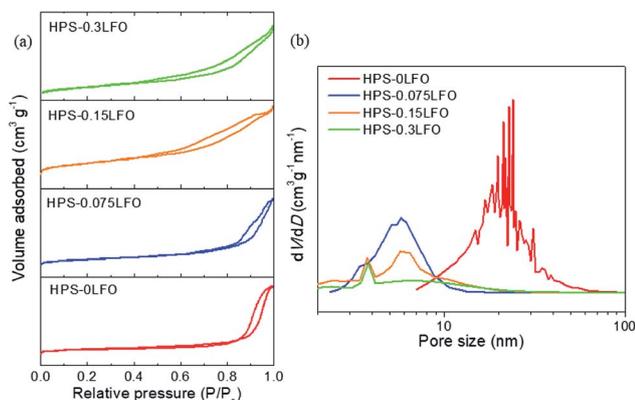Fig. 3 XRD patterns of HPS-xLFO (x = 0, 0.075, 0.15, 0.3) as compared with that of LFO.

Fig. 4 (a) N$_2$ adsorption–desorption isotherms and (b) BJH pore size distributions of HPS-xLFO (x = 0, 0.075, 0.15, 0.3).

The nitrogen adsorption–desorption isotherms and BJH pore size distribution curves of HPS-xLFO (x = 0, 0.075, 0.15, 0.3) are shown in Fig. 4. The N$_2$ adsorption–desorption isotherm curves of all samples showed a type IV isotherm with H2-hysteresis loops (Fig. 4a), which suggests the characteristic of mesoporous structure.[25] It can be seen from Fig. 4b that HPS possessed a broad pore size distribution with multimodal mesopores ranging from 15 nm to 30 nm. It is worth noting that the high BET surface area of 496.62 m^2 g^{-1} was recorded for HPS-0LFO; whereas that of HPS-xLFO (x = 0.075, 0.15, 0.3) was considerably reduced from 349.52 m^2 g^{-1} to 123.12 m^2 g^{-1} as the theoretical molar ratio of LFO loading to silica increased from 0.075 to 0.3. The pore volume of HPS-xLFO showed a similar trend, from 2.34 cm^3 g^{-1} (HPS-0LFO), 1.22 cm^3 g^{-1} (HPS-0.075LFO), 0.47 cm^3 g^{-1} (HPS-0.15LFO) to 0.27 cm^3 g^{-1} (HPS-0.3LFO). The decrease of BET surface area and total pore volume accompanied with the increase of LFO loading could be attributed to the presence of LFO in the pores and channels of the HPS support. These results suggest that LFO was successfully incorporated into the mesopores of HPS. A low BET surface area of 8.06 m^2 g^{-1} was observed for the LFO sample synthesized without the use of a HPS support. As can be seen, the LFO-doped HPS samples exhibited much higher specific surface area and presented accessible pores, providing more active sites and pathways for RhB removal.

Fig. S1† presents the UV-vis absorption spectra of HPS-doped LFO as compared with that of LFO. All samples exhibited the broad absorption peaks in the visible region, implying they could absorb visible light. Fig. 5 presents the bandgap values of LFO and HPS-xLFO (x = 0.075, 0.15, 0.3). They were estimated from the interception of the straight line fitted the curve $[F(R)h\nu]^2$ versus $h\nu$, in which $F(R)$ is the Kubelka–Munk function and $h\nu$ is the energy of the incident photon (shown in the inset of Fig. S1†). The corresponding bandgap was 2.21 eV, 2.31 eV, and 2.34 eV, respectively, for HPS-0.075LFO, HPS-0.15LFO, HPS-0.3LFO, which was narrower as compared with 2.36 eV for LFO. In the literature, Perathoner and co-workers also reported the improved effectiveness of light absorption of SBA15-supported TiO$_2$, relative to TiO$_2$.[34]

3.2 Adsorptive removal of RhB using HPS-xLFO

The photo-Fenton degradation of RhB generally takes place on the surface of catalyst; therefore the RhB adsorption capability of
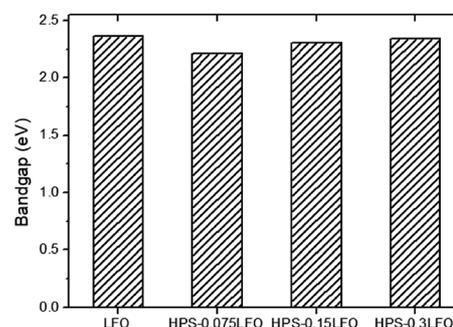

Fig. 5 Bandgap of HPS-xLFO (x = 0.075, 0.15, 0.3), as compared with that of LFO.
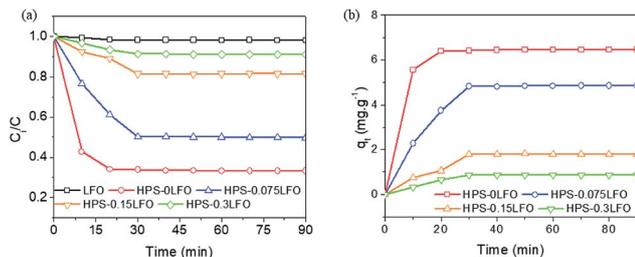
Fig. 6 (a) Removal of RhB *via* adsorption by using LFO or HPS-*x*LFO (x = 0, 0.075, 0.15, 0.3) (reaction conditions: temperature = 25 °C; initial RhB concentration = 10 mg L^{-1}; catalyst dosage = 1 g L^{-1}; pH = 6); (b) the corresponding RhB adsorption capacity.

LFO or HPS-*x*LFO (x = 0, 0.075, 0.15, 0.3) is expected to affect its photocatalytic performance.[24,35–37] Fig. 6a shows the adsorptive removal of RhB using LFO and HPS-*x*LFO (x = 0, 0.075, 0.15, 0.3), which was conducted in the dark for 90 min. Fig. 6b reveals the RhB adsorption capacity of the samples as a function of time.

The adsorption kinetics were not in good agreement with the pseudo-first-order model, as revealed by the low values of r^2 (r^2 = 0.8161–0.9862) in Table S1.† On the other side, high correlation coefficients (r^2 = 0.9661–0.9998; Table S1†) of the linear plots suggest the good agreement of the kinetic data with the pseudo-second-order model, which indicates the process is mainly chemisorption.

As shown above, the HPS-*x*LFO (x = 0, 0.075, 0.15, 0.3) samples exhibited better adsorption capability of RhB than LFO. This might be ascribed to their structural properties (specific surface area and porosity), which were seen in the SEM, TEM and nitrogen adsorption–desorption characterization. The porous structure of the HPS support (HPS-0LFO) was observed in the SEM and TEM images (Fig. 1 and 2), which could offer more space and pathways to facilitate the adsorption of RhB as compared with LFO solid crystals. Moreover, mesoporous silica material has an abundance of silanol groups (Si–OH) on the surface;[38,39] whilst RhB molecules contain carboxyl groups. A hydrogen bond might be established between the functional groups of the HPS support and RhB,[40] which would translate into higher RhB adsorption by HPS-*x*LFO than by LFO. HPS-0LFO exhibited the highest adsorption capacity as compared to other LFO-doped HPS samples (HPS-0.075LFO, HPS-0.15LFO and HPS-0.3LFO); since the doping of LFO into the HPS support reduced specific surface area, pore volume and number of surface silanol groups. The BET surface area and pore volume of the catalysts changed in a trend of HPS-0LFO > HPS-0.075LFO > HPS-0.15LFO > HPS-0.3LFO. This is consistent with the obtained results for RhB adsorption capability.

3.3 Photo-Fenton catalytic degradation of RhB using HPS-*x*LFO

To evaluate the photo-Fenton-like catalytic activity of HPS-*x*LFO (x = 0, 0.075, 0.15, 0.3), the degradation of RhB in the presence of H$_2$O$_2$ under visible light irradiation was carried out. The data were fitted with the pseudo-first-order kinetic model and the apparent rate constant was obtained from the slope of the straight line by plotting $-\ln(C_t/C_0)$ as a function of time.

Fig. S2† reveals no change in C_t/C_0 in the absence of catalyst and H$_2$O$_2$, implying that RhB does not be self decompose under visible light irradiation. Without the use of catalyst, approximately 7% of RhB was removed in the presence of H$_2$O$_2$ and visible light. A limited amount of RhB ($\sim$5%) was removed using just the catalyst of HPS-0.15LFO and exposure to visible light source. As compared with the results in Fig. 7, the use of H$_2$O$_2$ is indispensible for the efficient removal of RhB from water when using the as-prepared catalyst herein.

The photo-Fenton-like catalytic degradation of RhB using HPS-0.075LFO was 72.1%, which was slightly lower than that using LFO, which was 88.6%. The pseudo-first-order reaction constant of HPS-0.075LFO and HPS-0LFO was 0.0174 min^{-1} and 0.0215 min^{-1}, respectively. The relatively lower degradation performance of HPS-0.075LFO might be explained by the small loading of LFO into the HPS support resulting in fewer active sites available for degradation. When the molar ratio of LFO loading and silica was increased to 0.15 the RhB degradation efficiency of HPS-0.15LFO reached 97.5%, with the pseudo-first-order reaction rate constant 0.0423 min^{-1}. However, when using HPS-0.3LFO, the degradation efficiency was reduced slightly to 95.9% (the pseudo-first-order reaction rate constant was 0.0327 min^{-1}). This could be attributed to excess LFO partially covering or blocking the pores in the HPS support; as a result, the transport of organic into pores and subsequently its degradation was hindered.

Note that, the use of HPS-0.15LFO and HPS-0.3LFO resulted in better removal of RhB (97.5% and 95.9%, respectively) than LFO (88.6%) in the photo-Fenton degradation. In particular, the theoretical molar ratio of LFO/silica in HPS-0.15LFO and HPS-0.3LFO was 0.15 and 0.3. No degradation of RhB was found when using the HPS support (HPS-0LFO) as the catalyst, suggesting the support plays no role in degradation reaction. That implies that for the same dosage of catalyst, the actual amount of LFO in the doped HPS participating in the reaction was much smaller but its activity was more efficient, as compared with the bulk LFO crystals. On the other side, the RhB adsorption using HPS-0.15LFO or HPS-0.3LFO was noticeable in Fig. 6, in contrast to the negligible adsorption using the bulk LFO crystals. This suggests that both of the LFO-doped catalysts could adsorb RhB from solution onto the silica support and guarantee the degradation to occur smoothly on the LFO active sites.[24]

As can be seen above, the plain silica support HPS-0LFO could remove RhB to some level, mainly governed by
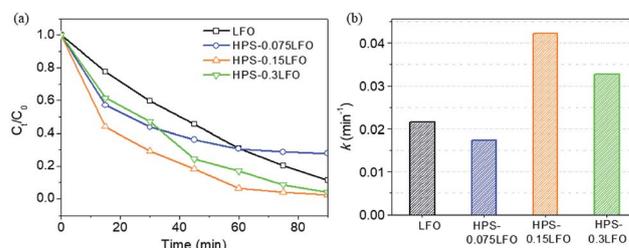

Fig. 7 (a) Removal of RhB in the photo-Fenton reaction using LFO or HPS-*x*LFO (x = 0.075, 0.15, and 0.3) and (b) corresponding degradation rate constants (reaction conditions: temperature = 25 °C, initial dye concentration = 10 mg L^{-1}, catalyst dosage = 1 g L^{-1}, initial H$_2$O$_2$ concentration = 10 mM and initial pH = 6).

adsorption (~65% shown in Fig. 6a). So far, various methods, including biological, physical and chemical ways, have been widely explored to remove organics and dyes from water. Adsorption, as a traditional method, only transfers dyes from water to another phase. It normally requires further treatment of saturated adsorbents after adsorption, *e.g.* disposal or regeneration. For example, in the case of this study, the use of high temperature (normally >500 °C) or organic solvent would be needed to regenerate dye-saturated adsorbents for recycle and reuse,[41,42] which may add further cost and complexity to the process. Advanced oxidation process (AOPs) have shown advantageous features as compared with adsorption. Especially, the heterogenous AOPs (*e.g.* photo-Fenton) has demonstrated promising results for degradation of dyes to produce more biologically degradable and less toxic substances.[43] In our study, the use of LFO doping onto HPS (*e.g.* HPS-0.15LFO) could achieve much better total removal rate of RhB (over 98%), as compared to only <75% using the parent HPS-0LFO. Note that, the regeneration process herein is simple and capable for scale-up; especially it required no high temperature calcination and organic solvent (the results of recycle and reuse were shown in 3.4.5). The photo-Fenton catalytic performance in terms of dye removal using HPS-0.15LFO was almost completely retained after 4 cycles of use.

Our work also compared the photo-Fenton catalytic performance of HPS-0.15LFO with that of Fe_2O_3-doped HPS using our HPS support (under the same molar ratio of loading). However, the preliminary results found that the degradation rate of plain Fe_2O_3 or its doped HPS was <70%, thus lower than that of HPS-0.15LFO. More systematic study is undertaken to reveal the reasons.

As discussed above, HPS-0.15LFO exhibited the greatest reaction rate constant, best degradation performance and highest removal efficiency, among the samples of LFO-doped HPS, HPS support and LFO pure crystals. Therefore, we selected HPS-0.15LFO to study the effects of catalyst dosage, H_2O_2 centration, initial pH and co-existing ions on photo-Fenton degradation of RhB.

Interestingly, in the dark, HPS-0.15LFO yielded a degradation rate of 66.5% (Fig. S2†), revealing that HPS-0.15LFO can act as a heterogeneous Fenton-like catalyst.[24] With the use of visible light, the degradation of RhB was significantly enhanced, up to 97.5%, strongly suggesting that the combination of HPS-0.15LFO catalyst, H_2O_2 and visible light is necessary to achieve efficient and effective removal of RhB.

3.4 Effect of operational parameters on photo-Fenton using HPS-0.15LFO

3.4.1 Effect of catalyst dosage. The impact of HPS-0.15LFO dosage on the RhB degradation was assessed in Fig. 8a. The increase of HPS-0.15LFO dosage from 0.5 g L^{-1} to 1.0 g L^{-1} led to the enhancement of degradation from 94.8% to 97.5%; whereas the degradation efficiency decreased to 96.1% when further increasing HPS-0.15LFO dosage up to 1.2 g L^{-1}. As can be seen clearly from Fig. 8b that the pseudo-first-order reaction rate constant k at different dosages followed the order: 0.5 g L^{-1}
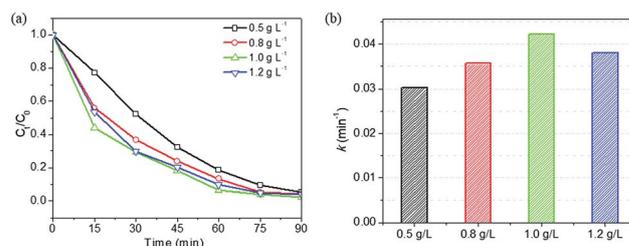

Fig. 8 (a) Effect of catalyst dosage on the removal of RhB in the photo-Fenton reaction and (b) degradation rate constants (reaction conditions: temperature = 25 °C, initial dye concentration = 10 mg L^{-1}, initial H_2O_2 concentration = 10 mM and initial pH = 6).

< 0.8 g L^{-1} < 1.2 g L^{-1} < 1 g L^{-1}. This can be explained by the increasing number of active sites for RhB degradation. However, further increase of catalyst dosage may limit the visible light transmission into the reaction suspension, and in turn lower visible light utilization and reduce photo-Fenton degradation efficiency. Therefore, 1 g L^{-1} was identified as the optimal catalyst dosage for photo-Fenton degradation of RhB using HPS-0.15LFO in our experiment.

3.4.2 Effect of H_2O_2 concentration. In the photo-Fenton-like catalytic degradation, H_2O_2 concentration has a great influence on the degradation of organic pollutants due to the fact that the amount of generated ˙OH radicals is governed by the concentration of H_2O_2.[44] The photo-Fenton catalytic degradation of RhB using HPS-0.15LFO in the presence of various concentrations of H_2O_2 is presented in Fig. 9a. It was observed that as the H_2O_2 concentration increased from 10 mM to 15 mM, the degradation efficiency of RhB was enhanced, reaching to 98.6%. However, further increase in H_2O_2 concentration did not considerably improve the degradation efficiency. The RhB degradation efficiency was 97.9% for the H_2O_2 concentration was 20 mM and this rate then decreased to 95.7% when increasing the H_2O_2 concentration up to 25 mM. The fittings of photo-Fenton catalytic degradation data in Fig. 9b illustrate that the pseudo-first-order reaction rate constants k for RhB degradation in 10 mM, 15 mM, 20 mM, and 25 mM H_2O_2 were 0.0423 min^{-1}, 0.0544 min^{-1}, 0.0486 min^{-1}, and 0.0380 min^{-1}, respectively.

It might be attributed to the scavenging effect because of excess H_2O_2, as shown in eqn (1):[45]
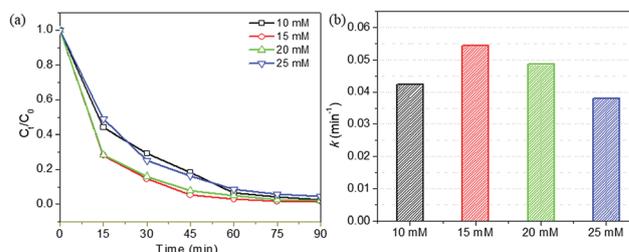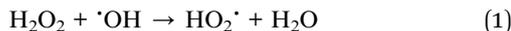

Fig. 9 (a) Effect of H_2O_2 on the removal of RhB in the photo-Fenton reaction and (b) degradation rate constants (reaction conditions: temperature = 25 °C, initial dye concentration = 10 mg L^{-1}, catalyst dosage = 1 g L^{-1} and initial pH = 6).

$$H_2O_2 + {}^{\bullet}OH \rightarrow HO_2{}^{\bullet} + H_2O \tag{1}$$

At high concentration of H_2O_2, H_2O_2 could act as a ${}^{\bullet}OH$ radical scavenger, resulting in the reduced number of ${}^{\bullet}OH$ radicals. Moreover, the generated $HO_2{}^{\bullet}$ would be less reactive than ${}^{\bullet}OH$;[46] as a result, the RhB degradation efficiency decreased. The optimal H_2O_2 concentration for the photo-Fenton degradation of RhB using HPS-0.15LFO was found to be 15 mM.

3.4.3 Effect of initial pH. The effect of initial solution pH on the degradation of RhB is presented in Fig. 10a. The experiment was conducted in the pH range of 4–9. Since textile industry wastewater is nearly neutral to slightly acidic,[47] the optimal pH in the photo-Fenton-like degradation of RhB using HPS-0.15LFO is of importance to determine cost effectiveness of process.
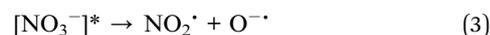
As reported in the literature,[48,49] the low degradation% of RhB at high pH might be attributed to the decomposition of H_2O_2 into less reactive hydroperoxyl radicals and the restriction of ${}^{\bullet}OH$ production in a basic medium. Moreover, in a solution with pH > 3.7 (pK_a of RhB), RhB presents in zwitterionic form.[26] At high pH, the zwitterionic form of RhB tends to form bigger molecules,[50] which might hinder the transport and entry of dye molecules into the pores of HPS-15LFO. In addition, the zwitterionic form of RhB molecules at high pH are less attackable by ${}^{\bullet}OH$ radicals.[26] These effects could explain the decrease in the degradation of RhB which was observed at high pH (e.g. pH > 6). Fig. 10b shows that the pseudo-first-order reaction rate constant k was the highest (0.0544 min^{-1}) at pH = 6; as compared with 0.0404 min^{-1}, 0.0346 min^{-1} and 0.0287 min^{-1} at pH = 7, 8 and 9, respectively. The maximum degradation efficiency of RhB (98.6%) was observed at pH = 6.

Note that the RhB degradation rate gradually decreased as the initial solution pH was reduced from 6 down to 4. Fig. 10b shows that the pseudo-first-order reaction rate constant k was 0.0369 min^{-1} and 0.0437 min^{-1}, respectively at pH = 4 and 5; which was smaller than that at pH = 6 (0.0544 min^{-1}), but still comparable or greater than those at pH > 6. Fig. S3† reveals the pH_{pzc} of HPS-15LFO to be 6.39, using pH drift method.[51–53] When the solution pH was below the pH_{pzc}, the surface of HPS-15LFO was positively charged; and above the pH_{pzc}, the surface was negatively charged. As the proton concentration increased at lower pH, RhB could be protonated to $RhBH^+$ under the

acidification with H^+.[54] The positively charged surfaces of HPS-0.15LFO might inhibit the adsorption of dye due to the repulsive force,[54] resulting in the observed slight decrease of degradation rate.

3.4.4 Effect of co-existing anions. As is well known, some of inorganic ions, including $NO_3{}^-$, $SO_4{}^{2-}$ and Cl^-, are common coexisting ions with dyes in real wastewater originated from dyestuff industries, which might affect the degradation of RhB using HPS-0.15LFO.

In Fig. 11a, the coexistence of $NO_3{}^-$ ion could slightly improve the degradation efficiency. Similar results were also reported by previous studies.[55,56] The pseudo-first-order reaction rate constant k was 0.0702 min^{-1} in the presence of 0.1 M $NaNO_3$. This may be explained by the photolysis of $NO_3{}^-$ to produce hydroxyl radicals via the following reactions:[57,58]

$$NO_3{}^- + h\nu \rightarrow [NO_3{}^-]^* \tag{2}$$

$$[NO_3{}^-]^* \rightarrow NO_2{}^{\bullet} + O^{-{\bullet}} \tag{3}$$

$$O^{-{\bullet}} + H_2O \rightarrow {}^{\bullet}OH + OH^- \tag{4}$$

The presence of Cl^- and $SO_4{}^{2-}$ showed an inhibitory effect on the RhB photo-Fenton catalytic degradation using HPS-0.15LFO. The pseudo-first-order reaction rate constant k was 0.0413 and 0.0280 min^{-1} when NaCl or Na_2SO_4 was added, in comparison of 0.0544 min^{-1} in the absence of coexisting ions. Eskandarloo et al. reported that Cl^- could act as an effective scavenging agent of holes and/or hydroxyl radicals,[59] thus lowering photo-Fenton-like catalytic degradation efficiency. This result is also in a good agreement with the literature.[60] Similarly, the inhibitory effect of $SO_4{}^{2-}$ on the degradation was suggested by Konstantinou and co-workers that $SO_4{}^{2-}$ react with h^+ and ${}^{\bullet}OH$ to form less reactive species $SO_4{}^{\bullet-}$ (eqn (5) and (6)):[61]

$$SO_4{}^{2-} + h^+ \rightarrow SO_4{}^{\bullet-} \tag{5}$$

$$SO_4{}^{2-} + {}^{\bullet}OH \rightarrow SO_4{}^{\bullet-} + OH^- \tag{6}$$
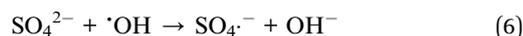
On the other side, the competitive adsorption could more or less contribute to the observed reduction of degradation rates. $SO_4{}^{2-}$, as the double charged anion, might be easier to adsorb on the surface of HPS-0.15LFO as compared to $NO_3{}^-$ and Cl^-,
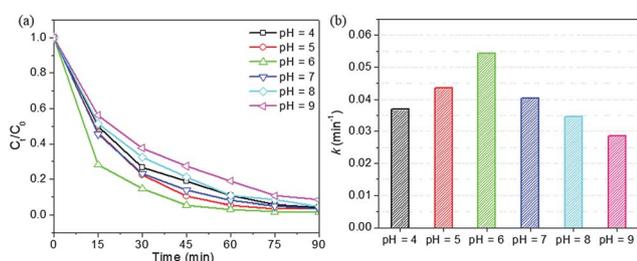

Fig. 10 (a) Effect of initial solution pH on the removal of RhB in the photo-Fenton reaction and (b) degradation rate constants (reaction conditions: temperature = 25 °C, initial dye concentration = 10 mg L^{-1}, catalyst dosage = 1 g L^{-1} and H_2O_2 concentration = 15 mM).
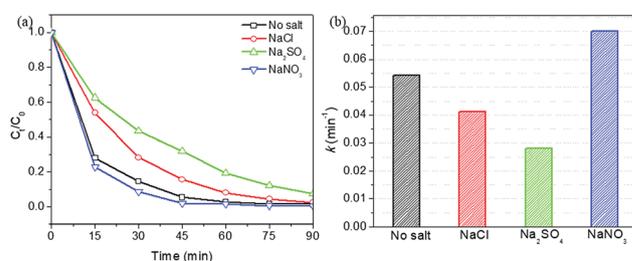

Fig. 11 (a) Effect of co-existing anions on removal of RhB in the photo-Fenton degradation and (b) degradation rate constants (reaction conditions: temperature = 25 °C, initial dye concentration = 10 mg L^{-1}, catalyst dosage = 1 g L^{-1}, H_2O_2 concentration = 15 mM, pH = 6, NaCl, $NaNO_3$ or Na_2SO_4 = 0.1 M).

which potentially blocked more active site and in turn reduced degradation rate more significantly.[56] The large molecular size of SO_4^{2-} might also enhance steric hindrance and reduce the contact of RhB with HPS-0.15LFO. Consequently, the degradation efficiency appeared slightly lower in the presence of SO_4^{2-} as compared with Cl^-.

3.4.5   Stability and reusability. To study the stability and reusability of HPS-0.15LFO, it was collected after the photo-Fenton catalytic reaction and reused in a subsequent reaction cycle. As illustrated in Fig. 12a, no significant loss of photocatalytic activity was seen within four cycles of photo-Fenton catalytic degradation. The XRD patterns of HPS-0.15LFO before and after four cycles of RhB degradation (in Fig. 12b) show no noticeable difference. These suggest that HPS-0.15LFO can be effectively recycled and reused repetitively without significant reduction in catalytic activity. The ICP-MS analysis showed that the concentration of La and Fe in the solution after degradation was 4.67 mg L^{-1} and 0.064 mg L^{-1}, respectively. The negligible concentration of dissolved ion detected implied that no significant contribution of homogeneous photo-Fenton reaction occurred. A slightly higher amount of dissolved La was detected; however, it did not play an essential role in contributing to catalytic degradation of RhB. The above results, including recycling use and XRD characterization, suggest the catalyst HPS-0.15LFO possessed good stability and reusability, thereby showing great potential for practical use in removing dyes and organics from wastewater.

3.4.6   Reaction mechanism. A possible mechanism for the photo-Fenton-like reaction using HPS-0.15LFO was proposed, as follows:
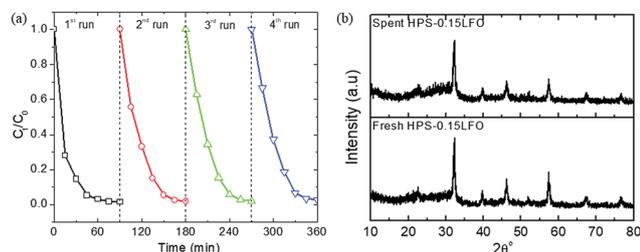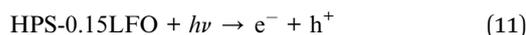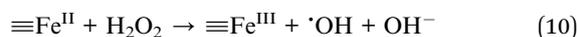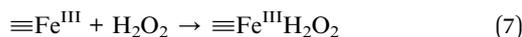
$$\equiv Fe^{III} + H_2O_2 \rightarrow \equiv Fe^{III}H_2O_2 \tag{7}$$

$$\equiv Fe^{III}H_2O_2 \rightarrow \equiv Fe^{II} + HO_2^\cdot + H^+ \tag{8}$$

$$\equiv Fe^{III} + HO_2^\cdot + H^+ \rightarrow \equiv Fe^{II} + O_2 + 2H^+ \tag{9}$$

$$\equiv Fe^{II} + H_2O_2 \rightarrow \equiv Fe^{III} + {}^\cdot OH + OH^- \tag{10}$$

$$HPS\text{-}0.15LFO + h\nu \rightarrow e^- + h^+ \tag{11}$$

$$H_2O_2 + e^- \rightarrow {}^\cdot OH + OH^- \tag{12}$$

Fig. 12 (a) Recycling use of HPS-0.15LFO for RhB removal in the photo-Fenton reaction (reaction conditions: temperature = 25 °C, initial dye concentration = 10 mg L^{-1}, catalyst dosage = 1 g L^{-1}, H_2O_2 concentration = 15 mM, pH = 6); (b) XRD patterns of the fresh HPS-0.15LFO before photo-Fenton-like catalytic degradation of RhB and the spent HPS-0.15LFO after four cycles of photo-Fenton-like catalytic degradation of RhB.
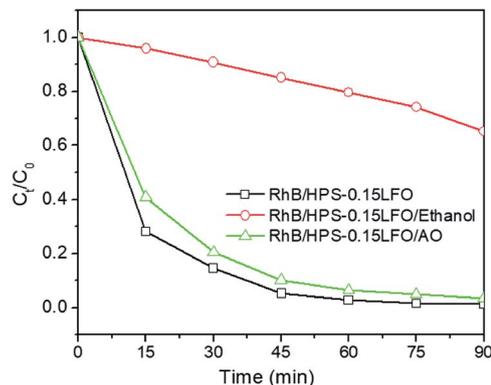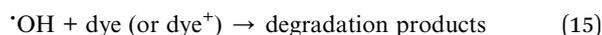

Fig. 13 Effect of ethanol and AO on the photo-Fenton-like catalytic degradation of RhB over HPS-0.15LFO (reaction conditions: temperature = 25 °C, initial dye concentration = 10 mg L^{-1}, catalyst dosage = 1 g L^{-1}, H_2O_2 concentration = 15 mM, pH = 6).

$$dye + h\nu \rightarrow dye^* \tag{13}$$

$$dye^* + h^+ \rightarrow dye^+ \tag{14}$$

$${}^\cdot OH + dye\ (or\ dye^+) \rightarrow degradation\ products \tag{15}$$

It is commonly accepted that the interfacial Fe atoms (denoted as $\equiv Fe^{III}$) of perovskite-based catalysts can activate H_2O_2 to form hydroxyl radicals (${}^\cdot OH$) during the Fenton-like reaction (eqn (7)–(10)).[8,62] The ${}^\cdot OH$ radical is considered as a strong oxidizing agent because of its standard redox potential (+2.8 V), which could oxidize most of the dyes to the mineral end-products.[63] Meanwhile, HPS-0.15LFO can absorb visible light to produce photogenerated electron–hole pairs (eqn (11));[64] the electron is trapped by H_2O_2 to generate highly reactive ${}^\cdot OH$ (eqn (12)) and the hole is also an important active species to directly mineralize organic (eqn (14)).[62] Note that the role of h^+ in oxidation process of organics has so far remained inconclusive.[65] Some studies speculated that h^+ could activate dye*, which was formed after light absorption of dye (eqn (13)), into dye$^+$ (eqn (14)); dye$^+$ or dye was then oxidized by ${}^\cdot OH$ radical (eqn (15)).[66,67]

To investigate the mechanism for photo-Fenton-like degradation over HPS-0.15LFO, the effect of active species, such as hole (h^+) and hydroxyl radicals (${}^\cdot OH$), in the process was explored. Ethanol and ammonium oxalate (AO) were selected for use as the scavengers of ${}^\cdot OH$ and h^+ in the trapping experiment, respectively.[68,69] Fig. 13 shows that when AO was introduced, no significant change was observed in the photo-Fenton catalytic RhB degradation. However, when ethanol was added into the reaction solution, the 90 min RhB degradation efficiency was suppressed to only 47.3%. It suggests that ${}^\cdot OH$ play a more significant role in the photo-Fenton-like catalytic RhB degradation using HPS-0.15LFO.

4.   Conclusions

The catalyst $LaFeO_3$ supported by mesoporous silica (HPS) was successfully synthesized by the method of impregnation and

subsequent calcination. The characterization results showed that the sample of HPS-0.15LFO with a theoretical LFO/silica molar ratio of 0.15 exhibited great surface area and a narrow bandgap. It exhibited higher total removal rate of RhB (98.9%) from water compared to the others with different loadings of LFO; which was contributed to dark adsorption (18.5% in 30 min) and photo-Fenton degradation (98.6% in 90 min in the presence of 15 mM H_2O_2, 1 g L^{-1} catalyst and pH of 6). The optimum operational conditions for photo-Fenton degradation using HPS-0.15LFO were found to be: RhB concentration = 10 mg L^{-1}, catalyst dosage = 1 g L^{-1}, pH = 6 and H_2O_2 = 15 mM. It is suggested that in this reaction, the hydroxyl radicals were the main active species. The high degradation efficiency, good reusability and stability may enable promising industrial application of HPS-0.15LFO as a visible-light-driven photo-Fenton-like catalyst for removal of organic from wastewater.

Conflicts of interest

There are no conflicts to declare.

Acknowledgements

Notes and references

1 E. Neyens and J. Baeyens, *J. Hazard. Mater.*, 2003, **98**, 33–50.
2 M. R. Carrasco-Díaz, E. Castillejos-López, A. Cerpa-Naranjo and M. L. Rojas-Cervantes, *Chem. Eng. J.*, 2016, **304**, 408–418.
3 K. Rusevova, F.-D. Kopinke and A. Georgi, *J. Hazard. Mater.*, 2012, **241**, 433–440.
4 M. Tekbaş, H. C. Yatmaz and N. Bektaş, *Microporous Mesoporous Mater.*, 2008, **115**, 594–602.
5 J. H. Ramirez, F. J. Maldonado-Hódar, A. F. Pérez-Cadenas, C. Moreno-Castilla, C. A. Costa and L. M. Madeira, *Appl. Catal., B*, 2007, **75**, 312–323.
6 H. Zheng, Y. Pan and X. Xiang, *J. Hazard. Mater.*, 2007, **141**, 457–464.
7 J. M. Chacón, M. T. Leal, M. Sánchez and E. R. Bandala, *Dyes Pigm.*, 2006, **69**, 144–150.
8 L. Ju, Z. Chen, L. Fang, W. Dong, F. Zheng and M. Shen, *J. Am. Ceram. Soc.*, 2011, **94**, 3418–3424.
9 J. An, L. Zhu, Y. Zhang and H. Tang, *J. Environ. Sci.*, 2013, **25**, 1213–1225.
10 Y. Nie, L. Zhang, Y.-Y. Li and C. Hu, *J. Hazard. Mater.*, 2015, **294**, 195–200.
11 L. Li, X. Wang and Y. Zhang, *Mater. Res. Bull.*, 2014, **50**, 18–22.
12 T. T. N. Phan, A. N. Nikoloski, P. A. Bahri and D. Li, *J. Ind. Eng. Chem.*, 2018, **61**, 53–64.
13 T. T. N. Phan, A. N. Nikoloski, P. A. Bahri and D. Li, *J. Environ. Chem. Eng.*, 2018, **6**, 1209–1218.
14 K. Rusevova, R. Köferstein, M. Rosell, H. H. Richnow, F.-D. Kopinke and A. Georgi, *Chem. Eng. J.*, 2014, **239**, 322–331.
15 K. Peng, L. Fu, H. Yang and J. Ouyang, *Sci. Rep.*, 2016, **6**, 19723.
16 K. Wang, H. Niu, J. Chen, J. Song, C. Mao, S. Zhang and Y. Gao, *Appl. Surf. Sci.*, 2017, **404**, 138–145.
17 P. Xiao, J. Hong, T. Wang, X. Xu, Y. Yuan, J. Li and J. Zhu, *Catal. Lett.*, 2013, **143**, 887–894.
18 H. Su, L. Jing, K. Shi, C. Yao and H. Fu, *J. Nanopart. Res.*, 2010, **12**, 967–974.
19 X. Ren, H. Yang, S. Gen, J. Zhou, T. Yang, X. Zhang, Z. Cheng and S. Sun, *Nanoscale*, 2016, **8**, 752–756.
20 S. Nguyen, V. Szabo, D. T. On and S. Kaliaguine, *Microporous Mesoporous Mater.*, 2002, **54**, 51–61.
21 J. Zhao, Y. Liu, X. Li, G. Lu, L. You, X. Liang, F. Liu, T. Zhang and Y. Du, *Sens. Actuators, B*, 2013, **181**, 802–809.
22 W. Huang, X. Yu, J. Tang, Y. Zhu, Y. Zhang and D. Li, *Microporous Mesoporous Mater.*, 2015, **217**, 225–232.
23 K. Zhang, L.-L. Xu, J.-G. Jiang, N. Calin, K.-F. Lam, S.-J. Zhang, H.-H. Wu, G.-D. Wu, B. l. Albela and L. Bonneviot, *J. Am. Chem. Soc.*, 2013, **135**, 2427–2430.
24 H. Li, J. Zhu, P. Xiao, Y. Zhan, K. Lv, L. Wu and M. Li, *Microporous Mesoporous Mater.*, 2016, **221**, 159–166.
25 S. Gai, P. Yang, L. Wang, C. Li, M. Zhang and L. Jun, *Dalton Trans.*, 2012, **41**, 4511–4516.
26 S. Merouani, O. Hamdaoui, F. Saoudi and M. Chiha, *Chem. Eng. J.*, 2010, **158**, 550–557.
27 S. K. Das, J. Bhowal, A. R. Das and A. K. Guha, *Langmuir*, 2006, **22**, 7265–7272.
28 H. M. Gad and A. A. El-Sayed, *J. Hazard. Mater.*, 2009, **168**, 1070–1081.
29 S. Sachdeva and A. Kumar, *J. Membr. Sci.*, 2009, **329**, 2–10.
30 K. Shakir, A. F. Elkafrawy, H. F. Ghoneimy, S. G. Elrab Beheir and M. Refaat, *Water Res.*, 2010, **44**, 1449–1461.
31 M. Faryadi, M. Rahimi and M. Akbari, *Korean J. Chem. Eng.*, 2016, **33**, 922–933.
32 W. Wei, S. Guo, C. Chen, L. Sun, Y. Chen, W. Guo and S. Ruan, *J. Alloys Compd.*, 2017, **695**, 1122–1127.
33 J. Chandradass and K. H. Kim, *Mater. Chem. Phys.*, 2010, **122**, 329–332.
34 S. Perathoner, P. Lanzafame, R. Passalacqua, G. Centi, R. Schlögl and D. S. Su, *Microporous Mesoporous Mater.*, 2006, **90**, 347–361.
35 W. Dong, C. W. Lee, X. Lu, Y. Sun, W. Hua, G. Zhuang, S. Zhang, J. Chen, H. Hou and D. Zhao, *Appl. Catal., B*, 2010, **95**, 197–207.
36 X. Li and J. Ye, *J. Phys. Chem. C*, 2007, **111**, 13109–13116.
37 J. Zhao, T. Wu, K. Wu, K. Oikawa, H. Hidaka and N. Serpone, *Environ. Sci. Technol.*, 1998, **32**, 2394–2400.
38 M. Kruk, M. Jaroniec and A. Sayari, *J. Phys. Chem. B*, 1997, **101**, 583–589.

39 J. M. Rosenholm, T. Czuryszkiewicz, F. Kleitz, J. B. Rosenholm and M. Lindén, *Langmuir*, 2007, **23**, 4315–4323.

40 P. Liao, Z. Malik Ismael, W. Zhang, S. Yuan, M. Tong, K. Wang and J. Bao, *Chem. Eng. J.*, 2012, **195–196**, 339–346.

41 P. Qin, Y. Yang, X. Zhang, J. Niu, H. Yang, S. Tian, J. Zhu and M. Lu, *Nanomaterials*, 2018, **8**, 4.

42 S. Wang, H. Li, S. Xie, S. Liu and L. Xu, *Chemosphere*, 2006, **65**, 82–87.

43 W. Wang, M. O. Tadé and Z. Shao, *Chem. Soc. Rev.*, 2015, **44**, 5371–5408.

44 J. Feng, X. Hu, P. L. Yue, H. Y. Zhu and G. Q. Lu, *Ind. Eng. Chem. Res.*, 2003, **42**, 2058–2066.

45 J. Feng, X. Hu, P. L. Yue, H. Y. Zhu and G. Q. Lu, *Water Res.*, 2003, **37**, 3776–3784.

46 R. Molina, F. Martínez, J. A. Melero, D. H. Bremner and A. G. Chakinala, *Appl. Catal., B*, 2006, **66**, 198–207.

47 I. Arslan-Alaton, G. Tureli and T. Olmez-Hanci, *J. Photochem. Photobiol.*, 2009, **202**, 142–153.

48 Y. Gao, H. Gan, G. Zhang and Y. Guo, *Chem. Eng. J.*, 2013, **217**, 221–230.

49 P. P. Gan and S. F. Y. Li, *Chem. Eng. J.*, 2013, **229**, 351–363.

50 G. Wang, J. Qi, S. Wang, Z. Wei, S. Li, J. Cui and W. Wei, *J. Dispersion Sci. Technol.*, 2017, **38**, 632–641.

51 P. Singh, P. Raizada, S. Kumari, A. Kumar, D. Pathania and P. Thakur, *Appl. Catal., A*, 2014, **476**, 9–18.

52 O. Bechambi, L. Jlaiel, W. Najjar and S. Sayadi, *Mater. Chem. Phys.*, 2016, **173**, 95–105.

53 J. R. Kim, S. G. Huling and E. Kan, *Chem. Eng. J.*, 2015, **262**, 1260–1267.

54 Y. Wang and W. Chu, *Ind. Eng. Chem. Res.*, 2011, **50**, 8734–8741.

55 X. Gao, X. Zhang, Y. Wang, S. Peng, B. Yue and C. Fan, *Chem. Eng. J.*, 2015, **273**, 156–165.

56 C. Wang, L. Zhu, M. Wei, P. Chen and G. Shan, *Water Res.*, 2012, **46**, 845–853.

57 L. Chu and C. Anastasio, *J. Phys. Chem. A*, 2003, **107**, 9594–9602.

58 X. Zhang, Y. Wang and G. Li, *J. Mol. Catal. A: Chem.*, 2005, **237**, 199–205.

59 H. Eskandarloo, A. Badiei and M. A. Behnajady, *Ind. Eng. Chem. Res.*, 2014, **53**, 6881–6895.

60 H.-c. Liang, X.-z. Li, Y.-h. Yang and K.-h. Sze, *Chemosphere*, 2008, **73**, 805–812.

61 I. K. Konstantinou and T. A. Albanis, *Appl. Catal., B*, 2004, **49**, 1–14.

62 L. Li, X. Wang, Y. Lan, W. Gu and S. Zhang, *Ind. Eng. Chem. Res.*, 2013, **52**, 9130–9136.

63 I. K. Konstantinou and T. A. Albanis, *Appl. Catal., B*, 2004, **49**, 1–14.

64 J. Yang, R. Hu, W. Meng and Y. Du, *Chem. Commun.*, 2016, **52**, 2620–2623.

65 W. Wang, M. O. Tadé and Z. Shao, *Chem. Soc. Rev.*, 2015, **44**, 5371–5408.

66 L. Li, X. Wang, Y. Lan, W. Gu and S. Zhang, *Ind. Eng. Chem. Res.*, 2013, **52**, 9130–9136.

67 Y. Soltanabadi, M. Jourshabani and Z. Shariatinia, *Sep. Purif. Technol.*, 2018, **202**, 227–241.

68 N. Daneshvar, D. Salari and A. Khataee, *J. Photochem. Photobiol. A*, 2003, **157**, 111–116.

69 S. Meng, D. Li, M. Sun, W. Li, J. Wang, J. Chen, X. Fu and G. Xiao, *Catal. Commun.*, 2011, **12**, 972–975.